Bjerknes Compensation at High Northern Latitudes: The Ocean Forcing the Atmosphere

E. VAN DER SWALUW, S. S. DRIJFHOUT, AND W. HAZELEGER

Royal Netherlands Meteorological Institute (KNMI), De Bilt, Netherlands

(Manuscript received 28 June 2006, in final form 21 February 2007)

ABSTRACT

The mechanisms for Bjerknes compensation of heat transport variations through the atmosphere and ocean on decadal time scales are investigated, using data output from a preindustrial control run of the Third Hadley Centre Coupled Ocean–Atmosphere General Circulation Model (HadCM3). It has recently been shown that Bjerknes compensation occurs on decadal time scales in a long preindustrial control run of HadCM3. This result is elaborated on by performing lead/lag correlations of the atmospheric and oceanic heat transports. By using statistical analysis, Bjerknes compensation is observed on decadal time scales at latitudes between 50° and 80°N. A maximum compensation rate of ~55% occurs at 70°N. At this latitude, the correlation rate peaks when the ocean leads the atmosphere by one year. The mechanisms by which Bjerknes compensation occurs at this latitude are investigated. Anomalies in oceanic heat transport appear to be associated with variations in the strength of the Atlantic meridional overturning circulation (MOC). The associated sea surface temperature (SST) anomalies are in general too weak to assert a significant impact on the atmosphere. At 70°N, however, such SST anomalies are a prelude to the transition from sea ice coverage to open water after which the associated changes in heat exchange with the atmosphere are strong enough to force an atmospheric response. Because of the presence of a strong MOC component in the Atlantic Ocean, this interaction is confined to the region where the northeast Atlantic and Arctic Oceans connect. The atmospheric response to increased (decreased) heating from below is a decreased (increased) poleward temperature gradient, leading to a decreased (increased) heat transport by baroclinic eddies. The anomalous thermal low that is set up by heating from the ocean is associated with anomalous advection of cold air from the Greenland landmass.

1. Introduction

The heat transport from the equator to the poles, through the atmosphere and the ocean, contributes to the maintenance of the quasi-equilibrium heat budget on earth. The total meridional heat flux can be calculated by integrating the observed net radiative fluxes (the difference between the absorbed shortwave minus the emitted longwave radiative flux) at the top of the atmosphere (TOA). To split up the total heat transport into its two components, one generally estimates the atmospheric heat transport from atmospheric observations and attributes the residual to the oceanic heat transport. Most studies use this indirect way of estimating the oceanic heat transport [however, see Wunsch (2005) for a reversed approach], since direct estimates from oceanic observations are sparse.

Trenberth and Caron (2001) presented estimates for the atmospheric and oceanic heat transports. Their results show a maximum value for the total heat transport of ~5 PW at 35° latitude. At this latitude 78% (92%) of the transport is accounted for by the atmosphere in the Northern (Southern) Hemisphere. However, as one moves from 35° latitude toward the tropics, the contribution from the oceanic component on the total heat transport increases and near the equator it is even larger than the atmospheric component. The latter is in agreement with a model for heat transport in the tropics proposed by Held (2001).

Although a lot of work has been performed to investigate poleward heat transport and the partitioning into its atmospheric and oceanic components, less attention has been paid to an equally important issue—that is, the variability of heat transport in both components. This is of importance since large anomalies in heat

Corresponding author address: E. van der Swaluw, Royal Netherlands Meteorological Institute (KNMI), P.O. Box 201, 3730 AE De Bilt, Netherlands.
E-mail: swaluw@knmi.nl

DOI: 10.1175/2007JCLI1562.1

transport could correspond to large climate shifts. The Held (2001) model for the heat transport in the tropics, mentioned above, argues that the circulation of the atmosphere and the ocean act in concert. This implies that in case of a circulation anomaly, the corresponding atmospheric and oceanic heat transport anomalies would have the same sign. However, variations in heat transport are expected to depend on circulation and stratification anomalies (Czaja and Marshall 2006); therefore, in general it is not apparent whether the sign of the atmospheric and oceanic heat transport anomalies is always the same in the model from Held (2001).

A different view was proposed by Bjerknes (1964). He argued that if the variations at the TOA energy flux and the heat storage of the ocean do not vary too much, large amplitude variations in the atmospheric and oceanic heat transports should be equal and of opposite sign so as to conserve total energy. Obviously this scenario strongly depends on the assumptions of a nearly constant TOA flux and ocean heat storage. The above scenario is now known as Bjerknes compensation. In recent work by Shaffrey and Sutton (2004, 2006) it was already shown that Bjerknes compensation occurs on decadal time scales and not on interannual time scales, because in the latter the variations at the TOA energy flux and the heat storage of the ocean do vary too much. Furthermore, Shaffrey and Sutton (2006) show the association between oceanic heat transport and variations in the meridional overturning circulation (MOC) on decadal time scales. They show that an increase (decrease) of the ocean heat transport/MOC strength yields higher (lower) sea surface temperature (SST) values in the Greenland–Iceland–Norwegian (GIN) Seas, which in turn yields a decrease (increase) in the meridional temperature gradient and therefore a reduced (enhanced) baroclinicity of the atmosphere. The latter corresponds with a weaker (stronger) atmospheric transient energy transport, hence yielding Bjerknes compensation. The variation of the MOC strength on decadal time scales is explained in Dong and Sutton (2005), who show that the latter is forced by the atmosphere, via the North Atlantic Oscillation (NAO).

We elaborate on the work by Shaffrey and Sutton (2006) by performing lead/lag correlations of the atmospheric and oceanic heat transports obtained from a preindustrial control run of a coupled climate model [Third Hadley Centre Coupled Ocean–Atmosphere General Circulation Model (HadCM3)]. At midlatitudes (40°–60°N) lead/lag correlations indicate that the atmosphere forces the ocean. At higher latitudes (60°–80°N) we find evidence that the ocean is forcing the atmosphere. In this paper we investigate in detail the mechanism by which Bjerknes compensation occurs, in particular at the northern high latitudes.

This paper is organized as follows. In section 2 we describe the occurrence of Bjerknes compensation on decadal time scales in a coupled climate model using lead/lag correlations and compensation rates, section 3 discusses the mechanism of how the ocean is forcing the atmosphere at high latitudes, leading to Bjerknes compensation, and in section 4 we summarize and present our conclusions.

2. Diagnostics: Bjerknes compensation

a. Heat transport in the Hadley Centre climate model

We used data from a preindustrial control run of HadCM3 from the archive of model output of the Intergovernmental Panel on Climate Change (IPCC). The choice for this state-of-the-art model was made because it has a realistic description of the Atlantic meridional overturning component (see below), which is important for a realistic description of Bjerknes compensation. Furthermore, it allows for a straight elaboration on the work from Shaffrey and Sutton (2006) who used the same model. In HadCM3 the atmospheric component has a resolution of 15 levels in the vertical and 2.5° latitude × 3.75° longitude, whereas the ocean component has a resolution of 20 levels in the vertical and 1.25° latitude × 1.25° longitude. The preindustrial control run we use consists of a total of 341 yr. We use a different run for our analysis than Shaffrey and Sutton (2006), who used a preindustrial control run of 93 decades, which is not available via the model output of the IPCC. The model simulates a maximum of 3.8 PW for the mean atmospheric heat transport in the Northern Hemisphere compared to values of ~4.5 PW [European Centre for Medium-Range Weather Forecasts (ECMWF)] and ~5.2 PW [National Centers for Environmental Prediction (NCEP)] given by Trenberth and Caron (2001). The maximum mean oceanic heat transport equals 1.4 PW in our model compared to ~1.6 PW (ECMWF) and ~2.1 PW (NCEP) from Trenberth and Caron (2001). The sea ice model in HadCM3 uses a simple thermodynamic scheme and behaves stable and realistic. The resolution of the HadCM3 model allows one to represent the channels in the Greenland–Iceland–Scotland (GIS) ridge, which is important to diagnose the formation and transport of North Atlantic Deep Water. Wood et al. (1999) have shown that the mean flow for the GIS ridge is 8.5 Sv (1 Sv $\equiv 10^6$ $m^3 s^{-1}$) in the HadCM3 model, which is a bit higher

than the observed estimate of 5.6 Sv. The strength of the meridional overturning circulation is stable and the model flow is 17.4 Sv at 24°N, which compares well with the observational estimate of 16–20 Sv (see, e.g., Talley et al. 2003; Bryden et al. 2005). There is a significant multidecadal variability, with an amplitude of 1–2 Sv, in the maximum Atlantic MOC and the model gives a reasonable quantitative simulation of the North Atlantic Deep Water. Further technical details of the HadCM3 model can be found in Gordon et al. (2000) and Wood et al. (1999).

We have calculated the global heat transport through the atmosphere H_{atm} following Shaffrey and Sutton (2006), by integrating the sum of the divergence of the zonally integrated surface flux from the ocean into the atmosphere F_{sfc}, and the energy flux coming in as radiation at the TOA F_{toa}. The global ocean heat transport H_{ocn} is obtained by integrating the divergence of the zonally integrated surface flux from the atmosphere into the ocean $-F_{\mathrm{sfc}}$, minus the time derivative of the oceanic heat content $\dot{Q}_{\mathrm{ocn}}$. Mathematically, we solve H_{atm} and H_{ocn} from the two equations below:

$$\frac{1}{a\cos\theta}\frac{\partial}{\partial\theta}(\cos\theta H_{\mathrm{atm}}) = \int_0^{2\pi}(F_{\mathrm{sfc}} + F_{\mathrm{toa}})a\cos\theta\, d\phi \quad \text{and} \quad \frac{1}{a\cos\theta}\frac{\partial}{\partial\theta}(\cos\theta H_{\mathrm{ocn}}) = -\int_0^{2\pi}(F_{\mathrm{sfc}} + \dot{Q}_{\mathrm{ocn}})a\cos\theta\, d\phi, \tag{1}$$

where a denotes the radius of the earth, θ is latitude, and ϕ is longitude. The integrand of both equations integrated over latitude from 90°S to 90°N yields a nonzero value. This arises because our method is based on calculating heat transport from fluxes rather than from the heat transport divergences, in which case model drift yields a residual. We correct for this by adding an area-dependent residual to the above set of equations such that calculating the above integrand again, we obtain exactly zero. The above procedure is carried out for each year independently. Furthermore, the calculated values for the heat transport are linearly detrended.

b. Bjerknes compensation

Our dataset consists of 341 samples of the annual mean of the atmospheric and oceanic heat transports as a function of latitude. The anomalies of these heat transports are expected to show Bjerknes compensation on decadal time scales, because at these time scales the TOA radiation flux and the heat storage of the ocean do not show large variations with respect to the variations in the heat fluxes of the atmosphere and the ocean (see, e.g., Bjerknes 1964; Shaffrey and Sutton 2006).

Throughout this paper we will apply a 15-yr running mean average to both components to emphasize decadal time scales. We take running mean averages of 15 yr, because the deviation from unity of this filter occurs at decades. To demonstrate Bjerknes compensation, we calculate the correlation coefficients between the atmospheric and oceanic heat transports as a function of latitude in the Northern Hemisphere. Figure 1a shows the result of these calculations. The atmospheric and oceanic heat transports are anticorrelated at most latitudes. The highest anticorrelation occurs close to 70°N and is −0.84. The anticorrelation between the atmospheric and oceanic heat transports shown at decadal time scales also occurs at annual time scales, but with significantly lower anticorrelation coefficients. This difference is indicating the validity of the assumptions made at the beginning of this section that Bjerknes compensation is operating at decadal time scales rather then at annual time scales. The apparent low compensation rate at annual time scales was already extensively discussed by Shaffrey and Sutton (2004).

Although these correlations give a qualitative indication for Bjerknes compensation, they do not yield a quantitative measurement. Therefore, we use the following recipe to define a compensation rate CR expressed in percentages, which will be applied to the 15-yr running mean samples of the atmospheric and oceanic heat transports. We define

$$\begin{aligned} |dH_{\mathrm{tot}}| &= |dH_{\mathrm{atm}} + dH_{\mathrm{ocn}}|, \\ W &\equiv \max(|dH_{\mathrm{atm}}|, |dH_{\mathrm{ocn}}|), \\ V &\equiv |dH_{\mathrm{tot}}|/W, \quad \text{and} \\ \mathrm{CR} &\equiv (1 - V) \times 100\%. \end{aligned} \tag{2}$$

The notation above is such that dH denotes the anomaly of the considered heat transport with respect to the mean value of all 341 samples for each latitude. Figure 1b shows the resulting compensation rate averaged over all 341 heat transport estimates with a run-

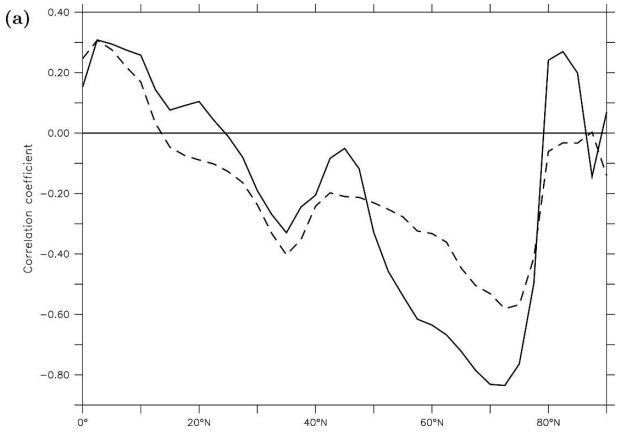

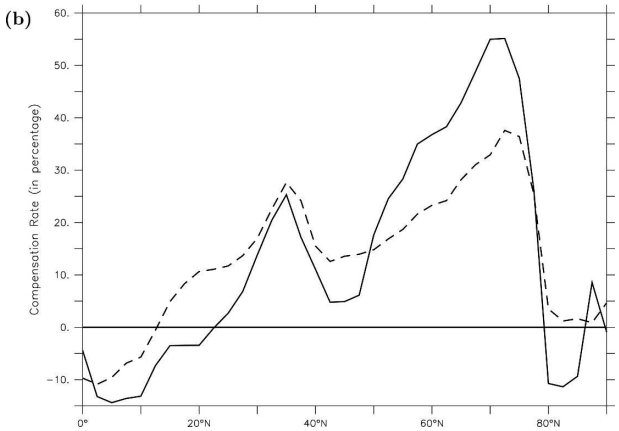

FIG. 1. (a) Correlation between atmospheric and oceanic heat transports. The solid line is calculated for samples with 15-yr running mean, whereas the dashed line is calculated for samples with annual means. (b) Compensation rate of the atmospheric and oceanic heat transport anomalies for a running mean of 15 (solid line) and 1 yr (dashed line).

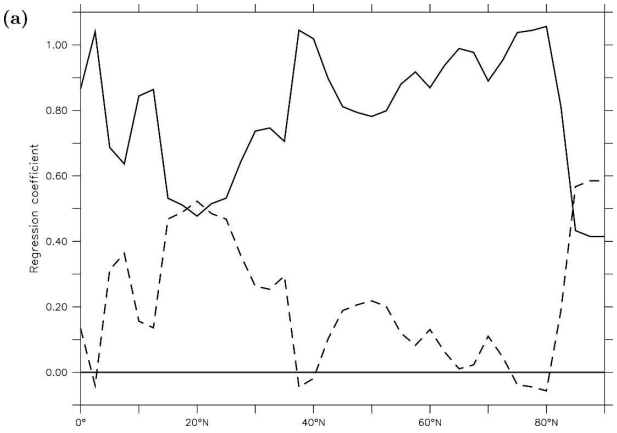

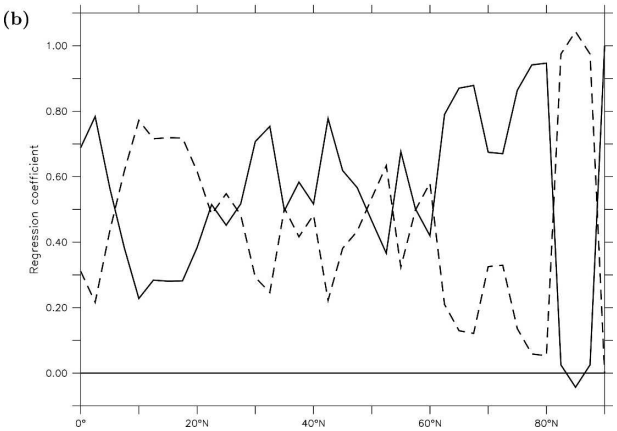

FIG. 2. (a) The linear regression of the divergence of the atmospheric heat transport onto the flux at the atmosphere–ocean interface (solid line) and the flux at the top of the atmosphere (dashed line). (b) The linear regression of the divergence of the oceanic heat transport onto the flux at the atmosphere–ocean interface (solid line) and the change of the ocean heat storage (dashed line). The regression coefficients are dimensionless in this figure.

ning mean of 15 yr and weighted with the amplitude of the anomalies. One can see that a maximum compensation rate of 55% is obtained at a latitude of 70°N for the samples with a running mean of 15 yr. The other line in this panel shows the compensation rate for the annual heat transport estimates. Comparing these two curves, one can clearly see that a significant increase in Bjerknes compensation occurs between 50° and 80°N by going from annual to decadal time scales.

We elucidate the above results by performing a linear regression of the divergence of the atmospheric heat transport [term on the left-hand side of Eq. (1)] onto the flux at the atmosphere–ocean interface and onto the flux at the top of the atmosphere [both terms are on the right-hand side of Eq. (1)]. The resulting regression coefficients are shown in Fig. 2a. Similarly we perform a linear regression of the divergence of the oceanic heat transport onto the flux at the atmosphere–ocean interface and onto the time derivative of the ocean heat storage. The resulting regression coefficients are shown in Fig. 2b. The two panels in Fig. 2 show that we observe a strong compensation mechanism between 60° and 80°N. It should be noted that the variations at the top of the atmosphere have an overall negligible influence on the heat budget. However, the ocean heat storage still has a significant influence on the heat budget outside of the region between 60° and 80°N.

Figure 3 is an extension of Fig. 1a by showing correlation coefficients between the atmospheric and oceanic heat transport anomalies on decadal time scales at different lags in time. The time axis is such that positive (negative) times indicate that the ocean (atmosphere) leads. The anticorrelation rate in Fig. 3 is highest at 70°N when the ocean leads the atmosphere by 1 yr. In

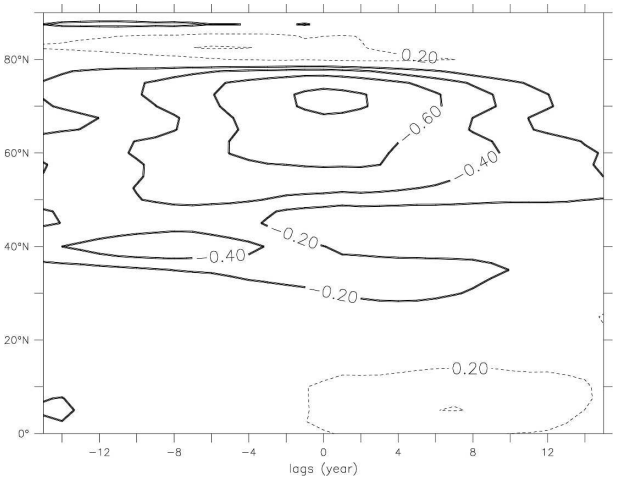

FIG. 3. Correlation between heat transport atmosphere and heat transport ocean with a 15-yr running mean. At positive lags the ocean is leading.

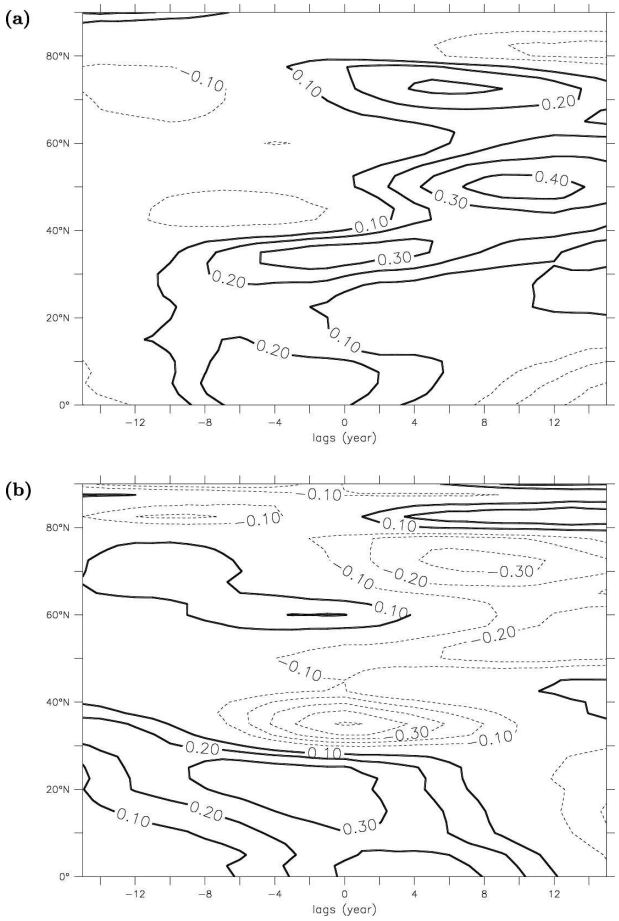

FIG. 4. The correlation of the (a) ocean heat transport and (b) atmospheric heat transport with the NAO index. At positive lags the NAO index is leading.

the rest of this paper we take this lead time of 1 yr as a reference value. We note, however, that the distribution of correlation rates shown in Fig. 3 are rather smooth around 70°N and that with the decadal averaging we applied, differences in lead times of the order of a few years are sometimes hard to distinguish. Furthermore, one can see clearly that for latitudes lower than 60°N, the highest anticorrelation coefficients are obtained when the atmosphere leads the ocean.

The fact that the atmosphere is leading the ocean at midlatitudes is probably related to the mechanism described by Dong and Sutton (2005, see their Fig. 12). They describe the interdecadal variability of the Atlantic MOC and suggest that the latter is stimulated by direct forcing of the atmosphere, via the NAO. Furthermore they show that although the forcing of the MOC variations is through an NAO-related wind stress curl and heat flux anomalies, the time scale of these variations is set by the oceanic circulation. These authors find a typical time scale of ~9 yr between forcing from the atmosphere and the subsequent response of the ocean, which is of the same order of magnitude as the lead time for which maximum correlation between atmosphere and ocean heat transports occurs from 40° to 60°N (Fig. 3). Note that their work was based on data analysis from a preindustrial control run of 1000 yr, with the same coupled atmosphere–ocean model as we consider here, that is, HadCM3.

We analyzed the connection between the atmospheric and oceanic heat transports and the NAO by calculating correlation coefficients. Figure 4a is consistent with Eden and Willebrand (2001), who show that there is a positive correlation between the NAO index and the ocean heat transport at 48°N (see their Fig. 3). Figure 4a shows a time scale of 10 yr at midlatitudes for the delay between the actual forcing from the atmosphere via the NAO and the subsequent response of the ocean—a similar time scale as the delayed baroclinic response mentioned by Eden and Willebrand (2001).

The negative lag correlation in Fig. 3 implies that a positive NAO phase is associated with decreased heat transport by the atmosphere at high latitudes. This apparently contradicts Carleton (1988), who finds that a positive NAO phase is associated with an increased heat transport by the atmosphere. In our model this specifically occurs in the tropics and subtropics (Fig. 4b) and obviously not in the mid- and high northern latitudes, since in that case there would be no Bjerknes compensation. Notice that Carleton (1988) shows strong longitudinally varying patterns at high latitudes (see, e.g., Figs. 5 and 6 of his paper), which do show negative correlation coefficients at higher latitudes of the North Atlantic Ocean (in his Figs. 5 and 6).

3. Oceanic response and forcing at 70°N

a. SST and heat flux from the ocean into the atmosphere

In the previous section, we have shown the occurrence of Bjerknes compensation at decadal time scales between 50° and 80°N, with a maximum compensation rate of 55% at 70°N. In this section we investigate why Bjerknes compensation is occurring at these latitudes and in particular why the compensation rate is showing a local maximum at 70°N. From the lead/lag correlations we infer that decadal oceanic heat transport variability leads the atmospheric heat transport variability at these latitudes, with maximum anticorrelation occurring at an ocean lead time of 1 yr. In this section we elucidate the mechanism that is responsible for this air–sea interaction.

In this and the next section we will consider a positive ocean heat transport anomaly and its consequences. The line of reasoning for the case of negative ocean heat transport anomalies is the same except for the sign of the correlation/regression coefficients. Previous work has already indicated that an increasing ocean heat transport is leading to an increase of the SST at northern midlatitudes (see, e.g., Shaffrey and Sutton 2006). We perform a linear regression of the ocean heat transport at 70°N with the SST to investigate the response of the latter to variations of the ocean heat transport at 70°N. We find that maximum values of the regression coefficient occur in the Greenland and Norwegian Seas, when the ocean heat transport at 70°N leads the SST in that region by 1 yr. Figure 5a shows the regression coefficient of SST on the ocean heat transport at 70°N for this specific time lag. Comparing the regression coefficients shown in Fig. 5a with the root-mean-square (RMS) variance of the SST in Fig. 5b, one can see that a large part, typically 50%, of the variance of the SST is coupled to the variations in the ocean heat transport at 70°N. The regression coefficients shown are normalized to a 0.01-PW variation in the ocean heat transport, obtained from the standard deviation of heat transport anomalies (not shown). One can see a maximum value of the regression coefficient of ~0.45 degree on a 0.01-PW heat transport variance. Inspection of Fig. 5a reveals that the SST response to heat transport variations across 70°N is mainly confined to the northeast Atlantic—in particular, the Norwegian and Greenland Seas in a latitude band between 70° and 80°N. Both the mean heat transport and its variability are low north of 80°N. Any variation in ocean heat transport across 70°N is associated with anomalous convergence of heat transport in the 70°–80°N latitude band. Such heat transport variations are likely associated with variations in the MOC (Dong and Sutton 2005). For this reason, variations in global ocean heat transport at 70°N display an SST imprint that is almost exclusively confined to the northeastern Atlantic. On a minor note, we observe a positive SST anomaly off Newfoundland in Fig. 5a, which we associate with a deviation of the strength and direction of the North Atlantic Current. This change in the North Atlantic Current also explains the negative anomaly in the Irminger and Labrador Seas.

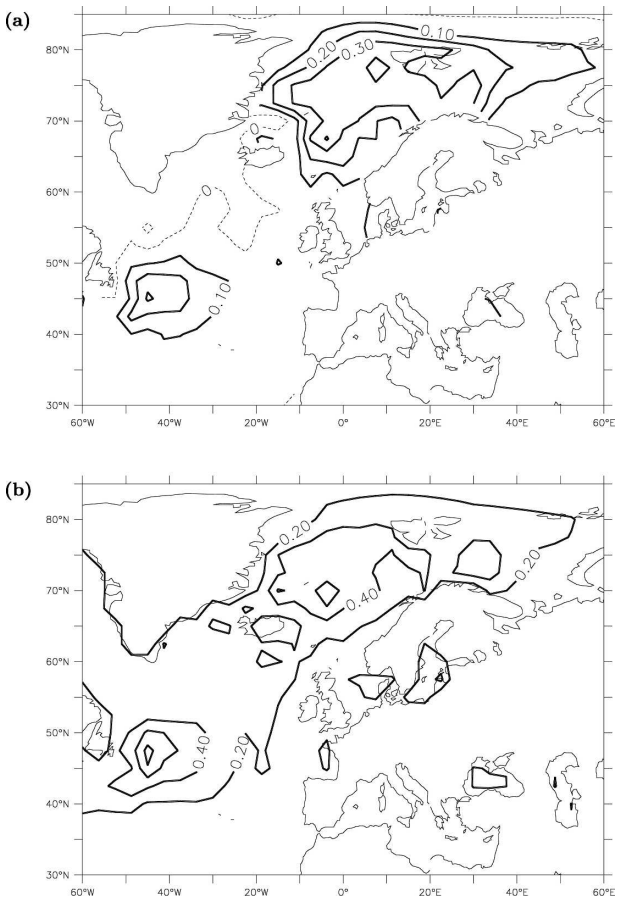

FIG. 5. (a) The linear regression of the SST (K) onto the normalized ocean heat transport at 70°N at a lag of 1 yr (ocean heat transport leads). We normalized the ocean heat transport with a value of 0.01 PW. (b) The standard deviation of the SST.

Ocean heat transport variations assert their impact on the atmosphere through a heat exchange between the interface dividing the atmosphere and ocean. A large fraction of the variance of the heat flux is coupled to the variations in the ocean heat transport at 70°N, with a maximum regression coefficient of 12 W m^{-2} per 0.01-PW heat transport variance (not shown) in the 70°–80°N latitude band. We investigated the relation between this heat exchange with ocean heat transport

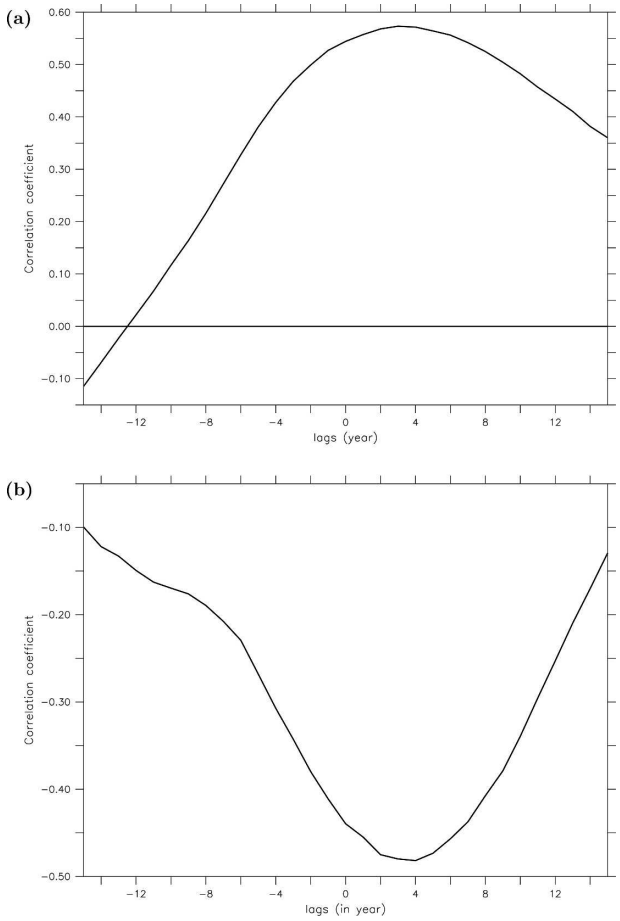

FIG. 6. (a) The correlation of the ocean heat transport at 70°N with the integrated flux of the ocean into the atmosphere in an area bounded by 70°W, 40°E, 60°N, and 80°N. (b) The correlation of the ocean heat transport at 70°N with the atmospheric eddy transport at 70°N. One can see that the ocean heat transport at 70°N leads in both cases by approximately 3 yr.

variations at 70°N by performing a lead/lag correlation between the ocean heat transport at this latitude and the heat flux from the ocean into the atmosphere zonally integrated between 70°W and 40°E and meridionally integrated between 60° and 80°N. The choice for this particular area was motivated by the results shown in Fig. 5a, that is, the region where the regression coefficients of the SST display maximum values. The result of this calculation is shown in Fig. 6a. It displays a maximum response of the heat flux when the ocean heat transport at 70°N is leading by 2–3 yr. We therefore conclude that the low-frequency atmospheric variability is forced by the ocean at 70°N. Notice that, although the ocean is forcing the atmosphere, the lead time of the ocean is slightly larger than the lead time found in section 2b.

The increase of the heat exchange at latitudes north of 70°N, when the oceanic heat transport increases, also leads to a decrease of the atmospheric heat transport at 70°N, according to the Bjerknes compensation displayed in Fig. 1. To gain more insight into the mechanisms that causes Bjerknes compensation at this latitude, we decompose the atmospheric heat transport into its mean meridional circulation component and eddy component. The total atmospheric heat transport is calculated by integrating the surface heat flux from the ocean and the TOA into the atmosphere, which yields the time-averaged total meridional transport of energy, that is, $[\overline{(gz + c_pT + L_vq)v}]$. The bar denotes time average, the square brackets denote the zonal average, and the three terms multiplied by the total meridional velocity v are respectively potential, internal, and latent energy. Next we calculate $g[\overline{v}\,\overline{z}] + c_p[\overline{v}\,\overline{T}] + L_v[\overline{v}\,\overline{q}]$, which subtracting from the time-averaged total meridional transport yields the transient synoptic eddies. We find that the transient synoptic eddy component dominates the variations in total atmospheric heat transport at this latitude (not shown). We do find the strongest correlation between the eddy component of the atmospheric heat transport and the ocean heat transport at 70°N when the latter leads by approximately 4 yr (see Fig. 6b). It is therefore concluded that Bjerknes compensation at 70°N is regulated by the transient eddy component in the atmospheric heat transport responding to variations in ocean heat transport. It is expected that a decrease of the transient eddy heat transport is coupled to a decrease of the baroclinicity of the atmosphere. This aspect is investigated in section 3b. The maximum anticorrelation rates found from Figs. 3 and 6 all indicate that the ocean is forcing the atmosphere at 70°N. However, they also show that it is not possible to allocate an exact response time of the atmosphere from the forcing by the ocean. They rather indicate that this time scale is of the order of a few years.

b. The atmospheric response

In Fig. 7a the correlation coefficients of the ocean heat transport at 70°N with dU/dp is shown. In Fig. 7b the regression coefficient of sea level pressure and the surface velocities onto the normalized heat transport at 70° are shown. Figures 7a and 7b both show maximum values for correlation and regression coefficients when the ocean heat transport variations at 70°N leads with 1 yr. In Fig. 7a one can see that when the ocean heat transport increases, dU/dp increases. This implies, using thermal wind balance, that dT/dy decreases and hence the baroclinicity of the atmosphere decreases. Obviously this is in agreement with the finding that the response of the atmospheric heat transport on ocean heat

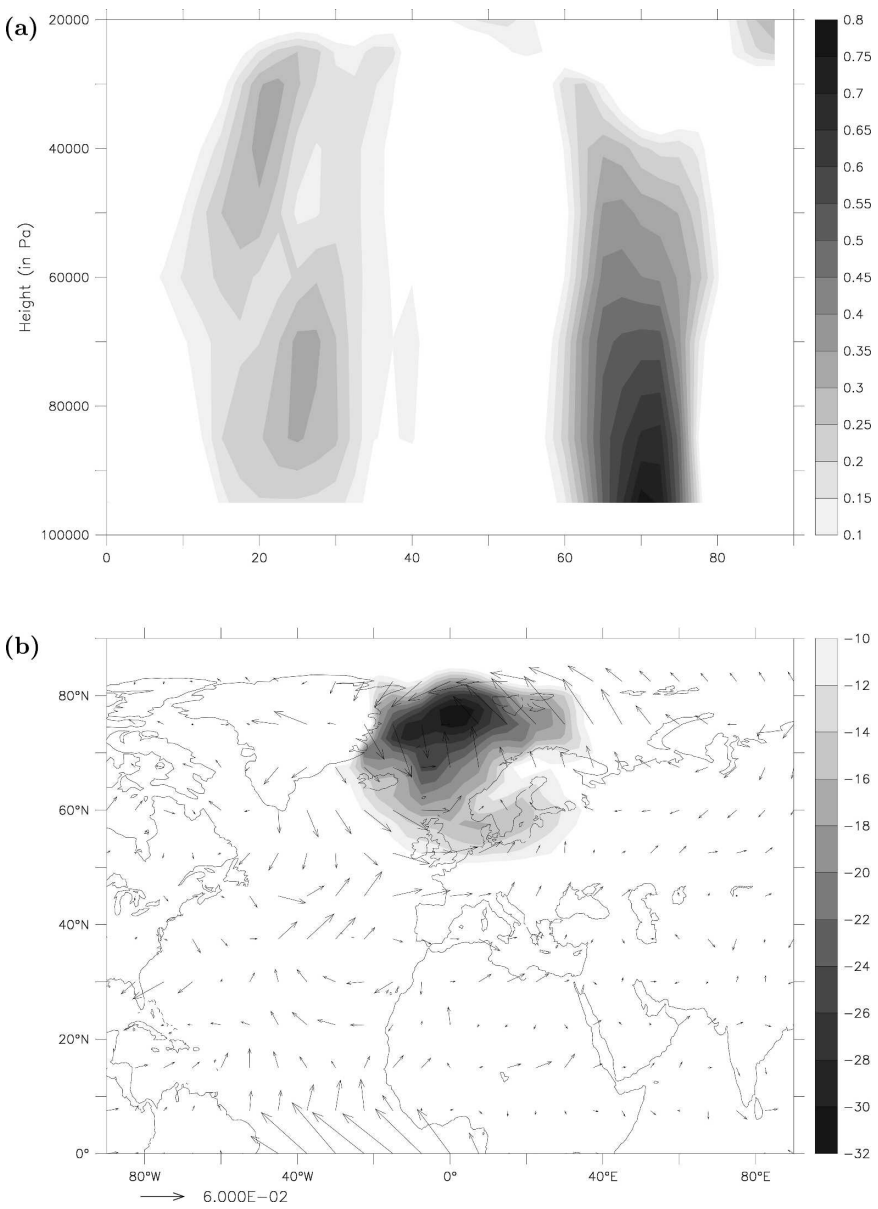

FIG. 7. (a) The correlation of the ocean heat transport at 70°N correlated with the vertical derivative of the zonal velocity. (b) The linear regression of the sea level pressure (Pa) and the surface velocities (m s^{-1}) onto the normalized ocean heat transport at 70°N. The ocean heat transport is normalized with a value of 0.01 PW. In both (a) and (b), the ocean heat transport leads by 1 yr.

transport variations occurs via its eddy component. Furthermore, we notice that Fig. 7a also indicates that the response of the atmosphere occurs in the lower troposphere. Figure 7b shows the influence of the increase of the baroclinicity of the atmosphere on the circulation, which shows a cyclonic anomaly in the region centered in the GIN Seas. The circulation anomaly is centered right above the SST anomaly shown in Fig. 5a and can be explained as the atmospheric response to the SST anomaly—that is, for positive SST anomalies, a thermal low.

The conclusion of section 3b is that in case of an increase of the ocean heat transport at 70°N, the baroclinicity of the atmosphere will decrease, because of an increase of the heat flux from the ocean into the atmosphere. It is obvious that the decrease of the baroclinicity of the atmosphere leads to a decrease of the heat transport through the atmosphere, since the eddy trans-

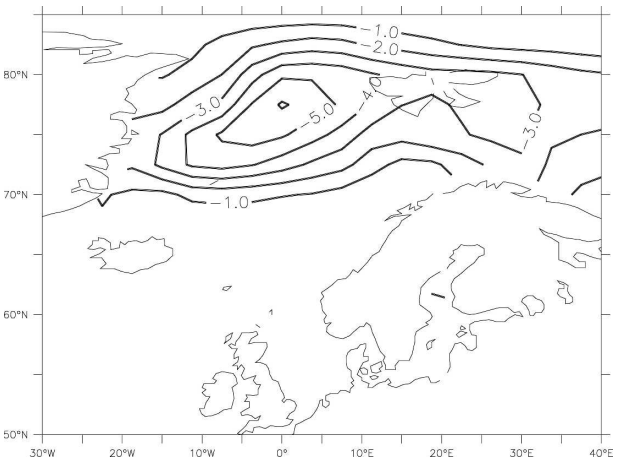

FIG. 8. The linear regression of the sea ice coverage (%) onto the normalized ocean heat transport at 70°N at a lag of 1 yr (ocean heat transport leads). The ocean heat transport is normalized with a value of 0.01 PW.

port variations dominate the atmospheric heat transport variations at 70°N. This implies a dampening of variations of radiation at the top of the atmosphere.

c. The particularity of 70°N: The role of sea ice

Figure 8 shows the regression coefficient between the ocean heat transport at 70°N and sea ice coverage when the ocean leads by 1 yr. Comparing the value of these regression coefficients with the RMS value of the sea ice coverage (not shown), we infer that the variability of the sea ice coverage in the region is mainly due (~75%) to variations in the ocean heat transport at 70°N. This result helps us to understand why the compensation rate at 70°N has its maximum value (Fig. 1b): the heat exchange between the ocean and the atmosphere scales with the temperature gradient at the interface dividing the ocean and the atmosphere. Because of the sea ice coverage, the surface air temperature and the SST are not coupled; hence the difference between both temperatures can be large. At the same time, the presence of sea ice prevents large heat fluxes between the atmosphere and the ocean. However, at those regions where occasionally transitions take place from coverage by sea ice to open water and vice versa, the large temperature gradient will lead to large heat fluxes between the ocean and atmosphere during these transition times. The region where most of the transitions from sea ice coverage to open water (and vice versa) takes place is the latitude band of 70°N, the latitude where Bjerknes compensation reaches its maximum compensation rate. Obviously the 70°N latitude band is not the only place where ocean heat transport and MOC variations are associated with SST anomalies. However, in general the associated heat flux anomaly is too small to assert a significant impact on the atmosphere, because of the strong coupling between extratropical SST and surface air temperature anomalies on decadal time scales (Drijfhout et al. 2001). It is only in regions where SST anomalies invoke changes from sea ice coverage to open water that the ocean–atmosphere heat flux can become large enough to yield a significant atmospheric response. The importance of the ocean heat transport on sea ice coverage and therefore on climate was already emphasized by Winton (2003). Furthermore, Poulsen et al. (2001) raises similar issues in another context, that is, the Neoproterozoic "snowball Earth." Also, our work is in line with the direct response of SST anomalies onto the atmosphere as reported by Deser et al. (2004). They also find an adaption of the baroclinic structure in the atmosphere associated with an equivalent barotropic thermal low caused by a positive SST anomaly.

From the above analysis we conclude that at latitudes ~70°N, the increase of the ocean heat transport leads to an increase of the SST. Subsequently, the increase of the SST yields a lower sea ice coverage, which in turn yields an increase of the heat flux from the ocean into the atmosphere. This heat flux is large enough to yield a significant atmospheric response due to the sea ice coverage, which prevents a direct coupling between SST and surface air temperature.

4. Discussion and conclusions

We calculated the atmospheric and oceanic heat transports for a 341-yr run of the coupled climate model HadCM3. We have shown that in the Northern Hemisphere Bjerknes compensation occurs on decadal time scales between 50° and 80°N with a maximum compensation rate of 55% at 70°N. We have elucidated the mechanism by which Bjerknes compensation operates at high latitudes, where the low-frequency oceanic variability forces the atmospheric variability. Although we studied Bjerknes compensation only in the HadCM3 model, we expect the general mechanism as explained here to be robust and valid in other climate models. The reason for this is that Bjerknes compensation is governed by quasigeostrophic dynamics associated with an increase/decrease of the meridional temperature gradient near the sea surface. Such a dynamic response, involving thermal wind balance, is quite general. Obviously in other models the exact position of deep-water formation areas will differ, as will the variations in sea ice coverage. For instance, in the present model the inflow of warm water into the Nordic seas is somewhat too large; therefore the thermal response east of

Greenland, which dominates Bjerknes compensation in this model, might be overestimated while on the other hand the role of the Labrador Sea might be underestimated. However, these changes will not change the global physical mechanism as elucidated in this paper to obtain Bjerknes compensation. Our most important results are summarized below.

- The maximum correlation rate between the atmospheric and oceanic heat transport variations occurs at 70°N when the ocean leads the atmosphere by 1 yr, but the exact lead time is difficult to estimate. In all of our analyses the highest anticorrelation rates always occur when the ocean leads the atmosphere. Moreover, a physical mechanism is shown that backs the statistical analysis, confirming the conclusion that the *ocean forces the atmosphere* at 70°N.
- The increase of the ocean heat transport at 70°N leads to an increase of the SST and a decrease of the sea ice coverage in the Greenland and Norwegian Seas. The combination of increasing SST and decreasing sea ice coverage yields an increase of the air–sea surface heat flux, which in turn decreases the poleward temperature gradient in the atmosphere.
- The increase of the air–sea surface heat flux in the Greenland and Norwegian Seas yields a thermally forced cyclonic pressure anomaly in the same area, which results in increased advection of cold air toward the Irminger Sea.
- The increased ocean heat transport is associated with decreased poleward temperature gradient in the atmosphere. As a result, the associated decrease of the atmospheric baroclinicity leads to a decrease of the atmospheric heat transport by baroclinic eddies. Since this atmospheric heat transport anomaly is of opposite sign with respect to the initial oceanic heat transport anomaly, we have Bjerknes compensation.

Acknowledgments. We acknowledge the international modeling groups for providing their data for analysis, the Program for Climate Model Diagnosis and Intercomparison for collecting and archiving the model data, the JSC/CLIVAR Working Group on Coupled Modeling and their Coupled Model Intercomparison Project and Climate Simulation Panel for organizing the model data analysis activity, and the IPCC WG1 TSU for technical support. The IPCC Data Archive at Lawrence Livermore National Laboratory is supported by the Office of Science, U.S. Department of Energy. EvdS is thankful for financial support from the BSIK project funded by NWO.

REFERENCES

Bjerknes, J., 1964: Atlantic air-sea interaction. *Advances in Geophysics,* Vol. 10, Academic Press, 1–82.

Bryden, H. L., H. R. Longworth, and S. A. Cunningham, 2005: Slowing of the Atlantic meridional overturning circulation at 25°N. *Nature,* **438,** 655–657.

Carleton, A. M., 1988: Meridional transport of eddy sensible heat in winters marked by extremes of the North Atlantic Oscillation, 1948/49–1979/80. *J. Climate,* **1,** 212–223.

Czaja, A., and J. Marshall, 2006: The partitioning of poleward heat transport between the atmosphere and ocean. *J. Atmos. Sci.,* **63,** 1498–1511.

Deser, C., G. Magnusdottir, R. Saravanan, and A. Phillips, 2004: The effects of North Atlantic SST and sea ice anomalies on the winter circulation in CCM3. Part II: Direct and indirect components of the response. *J. Climate,* **17,** 877–889.

Dong, B., and R. T. Sutton, 2005: Mechanism of interdecadal thermohaline circulation variability in a coupled ocean–atmosphere GCM. *J. Climate,* **18,** 1117–1135.

Drijfhout, S. S., A. Kattenberg, R. J. Haarsma, and F. M. Selten, 2001: The role of the ocean in midlatitude, interannual-to-decadal-timescale climate variability of a coupled model. *J. Climate,* **14,** 3617–3630.

Gordon, C., C. Cooper, C. A. Senior, H. Banks, J. M. Gregory, T. C. Johns, J. F. B. Mitchell, and R. A. Wood, 2000: The simulation of SST, sea ice extents and ocean heat transports in a version of the Hadley Centre coupled model without flux adjustments. *Climate Dyn.,* **16,** 147–168.

Eden, C., and J. Willebrand, 2001: Mechanism of interannual to decadal variability of the North Atlantic circulation. *J. Climate,* **14,** 2266–2280.

Held, I. M., 2001: The partitioning of the poleward energy transport between the tropical ocean and atmosphere. *J. Atmos. Sci.,* **58,** 943–948.

Poulsen, C. J., R. T. Pierrehumbert, and R. L. Jacob, 2001: Impact of ocean dynamics on the simulation of the Neoproterozoic "snowball Earth." *Geophys. Res. Lett.,* **28,** 1575–1578.

Shaffrey, L. C., and R. T. Sutton, 2004: The interannual variability of energy transports within and over the Atlantic Ocean in a coupled climate model. *J. Climate,* **17,** 1433–1448.

——, and ——, 2006: Bjerknes compensation and the decadal variability of the energy transports in a coupled climate model. *J. Climate,* **19,** 1167–1181.

Talley, L. D., J. L. Reid, and P. E. Robbins, 2003: Data-based meridional overturning streamfunctions for the global ocean. *J. Climate,* **16,** 3213–3226.

Trenberth, K. E., and J. M. Caron, 2001: Estimates of meridional atmosphere and ocean heat transports. *J. Climate,* **14,** 3433–3443.

Winton, M., 2003: On the climatic impact of ocean circulation. *J. Climate,* **16,** 2875–2889.

Wood, R. A., A. B. Keen, J. F. B. Mitchell, and J. M. Gregory, 1999: Changing spatial structure of the thermohaline circulation in response to atmospheric CO_2 forcing in a climate model. *Nature,* **399,** 572–575.

Wunsch, C., 2005: The total meridional heat flux and its oceanic and atmospheric partition. *J. Climate,* **18,** 4374–4380.